Available online at www.sciencedirect.com
SCIENCE DIRECT
Catalysis Today 105 (2005) 385–390
CATALYSIS TODAY
www.elsevier.com/locate/cattod

Hydrodynamic properties of a novel 'open wall' monolith reactor

J.J.W. Bakker [a,*], M.T. Kreutzer [a], K. de Lathouder [a], F. Kapteijn [a], J.A. Moulijn [a], S.A. Wallin [b]

[a] *Reactor and Catalysis Engineering, DelftChemTech, Delft University of Technology, Julianalaan 136, 2628 BL Delft, The Netherlands*
[b] *Core R&D, The Dow Chemical Company, 1776 Building, Midland, MI 48674, USA*

Abstract

The hydrodynamic behavior of high-porosity ceramic acicular mullite (ACM) monoliths operated in gas–liquid Taylor flow was investigated by cold-flow tracer residence time distribution (RTD) experiments and compared with the hydrodynamic behavior of classical cordierite monoliths in terms of static liquid fraction, maldistribution and mass exchange between the dynamic liquid zone and the static liquid zone. The piston-dispersion-exchange (PDE) model was successfully fitted to the experimental data. The multiphase fluid mechanics were indeed different for ACM and cordierite monoliths: in contrast to the classical cordierite system, the mass exchange between static liquid and dynamic liquid was much higher and the liquid phase could access the open volume of the permeable ACM monolith wall. On the other hand, the larger velocity maldistribution, larger static liquid fraction and the liquid interaction between adjacent ACM microchannels resulted in less plug flow behavior.

Keywords: Structured reactor; RTD; Hydrodynamics; Multiphase flow; Monoliths; Acicular mullite; Taylor flow

1. Introduction

Monolithic catalysts are used nowadays for various gas phase applications (e.g., in the automotive industry) and as an alternative for solid catalyzed gas–liquid reactions [1–5]. The advantages of using monolithic catalysts include low-pressure drop [6–8], ease of scale-up [2,9], high mass transfer rates [10–12], low-axial mixing [13] and elimination of a separation step [2].

''Classical'' ceramic monoliths for automotive applications are made of cordierite, and are used as structured supports for different catalytically active materials. A monolith consists of many millimeter sized parallel straight microchannels, separated by thin walls. On these walls, a washcoat (e.g., silica, γ-alumina or carbon) can be deposited with a high specific surface area. On this washcoat the catalytic phase, usually a precious metal, is dispersed [14,15].

A new type of monolith was synthesized by the Dow Chemical Company and consists of high-porosity acicular mullite (ACM) [16,17]. This ACM monolith distinguishes itself from a cordierite monolith by the permeability of the micro-structured walls. In contrast to the cordierite walls, the walls of the ACM monoliths are made up of an open network of interlocking elongated ceramic grains with lengths and diameters in the micrometer range. The ceramic grain size and the pore diameter size are tunable [16]. Fig. 1 shows two SEM micrographs of the ACM monolith walls with different ceramic grain sizes and pore diameters.

There are two possibilities to exploit the unique features of ACM monoliths: (i) for fast reactions that suffer from diffusional limitations, the deposition of a thin conformal catalyst layer (<1 μm) on the ACM grains maintains the open structure of the walls and minimizes the diffusional limitations and (ii) for reactions where mass transfer is not a limiting factor, the high porosity of the ACM monolith walls allows the catalyst loading per unit volume to be maximized [18].

The most important flow regime for co-current gas–liquid reactions in small diameter channels is Taylor flow (also

* Corresponding author. Tel.: +31 15 278 6733.
E-mail address: j.j.w.bakker@tnw.tudelft.nl (J.J.W. Bakker).

0920-5861/$ – see front matter © 2005 Elsevier B.V. All rights reserved.
doi:10.1016/j.cattod.2005.06.027

Nomenclature

$E(\theta)$	dimensionless residence time distribution
ka	mass transfer group (exchange between static and dynamic liquid) (s^{-1})
L	length of the monolith column (m)
N	dimensionless mass transfer parameter based on the PDE model
P	dimensionless dispersion parameter based on the PDE model
SLF	static liquid fraction based on the PDE model
u_G	superficial gas velocity (m/s)
u_L	superficial liquid velocity (m/s)
u_{TP}	total superficial velocity (m/s)

Greek letters

ε_L	total liquid holdup

called bubble-train flow or segmented flow) [19,20]. Taylor flow is a two-phase co-current flow pattern where the gas and liquid move consecutively through the channels as separate slugs. This two-phase flow pattern is observed in capillaries and monoliths [21–25]. The recirculation inside liquid slugs enhances radial mass transfer and a thin ''static'' liquid film, typically ranging in thickness from 5 to 50 μm between the wall and the bubble train, forms a small but noticeable barrier for the mass transfer rate in gas–liquid operated monolith channels. Hence, this flow pattern exhibits excellent mass transfer characteristics [10,26,27]. Moreover, backmixing is suppressed by the presence of bubbles when compared to single-phase laminar flow. Axial mixing is only possible inside the channels of a cordierite monolith by the diffusion into and out of the thin liquid film. However, for successful use of monolithic structures in multiphase reactions a uniform gas–liquid distribution is critical, because redistribution inside these structures is not possible. If the gas–liquid distribution over the top of the monolith entrance or if channel geometry is not perfect, the gas and liquid holdup and superficial velocities will vary from channel to channel, thereby adding a convective maldistribution term to the two-zone description of axial mixing [28].

The objective of this study was to determine the hydrodynamic behavior of the bare and coated ACM monoliths operated in co-current two-phase downflow, and to compare the hydrodynamic behavior of the ACM monoliths with ''classical'' cordierite monoliths.

2. Experimental

2.1. Materials

ACM monoliths of 15.5 cm in length and 4 cm in diameter with a cell density of 400 cpsi (mean channel diameter is 1 mm) were prepared by a proprietary Dow process to produce monoliths with medium (labeled as ACM-M) and large (labeled as ACM-L) elongated grains made of mullite. The wall thickness is 0.24 mm and the wall porosity is 60% for both ACM types with an average pore size of 9 and 16 μm for ACM-M and ACM-L, respectively. ACM-L monoliths were also coated (labeled as ACM-LC) with a colloidal silica layer, representative of a catalyst support, to see if the coating would influence the hydrodynamic behavior. The silica coating was prepared by dipping pre-treated ACM-L monoliths for 2 min, with a constant immersion speed and withdrawal speed of 5 mm/s, into a diluted Ludox® SM-30 (Adrich®) solution containing colloidal silica particles of 7 nm in diameter. After rotational drying and calcinations, a homogenous silica coating distributed on the mullite grains resulted, with a calculated layer thickness of around 500 nm leaving the 'open' wall structure of the ACM-L samples intact. Cordierite monoliths of equal outer dimensions and cell density (mean channel diameter is 1.1 mm) were used for comparison. The wall thickness of the cordierite samples is 0.18 mm with a wall porosity of 30% (average pore size is 2.7 μm). Water and air were used as fluids for all experiments.

3. Method

Cold-flow water–air RTD experiments in monoliths under Taylor flow were performed in a downflow configuration by introducing a pulse of a colored dye (Ecoline blue

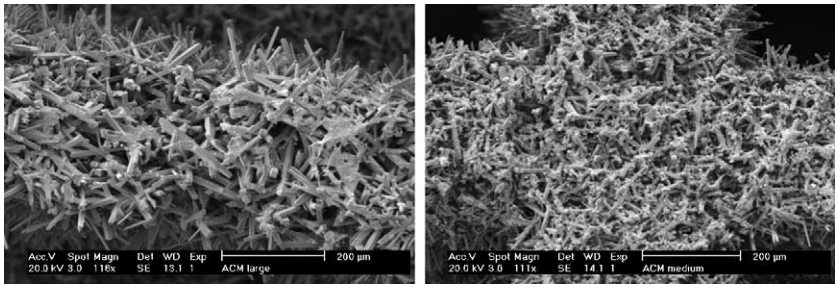

Fig. 1. SEM micrographs of the grain structure of ACM monolith walls. The left micrograph shows an ACM monolith wall with large ceramic grains (average grain length around 150 μm with an aspect ratio of 15). The right micrograph shows an ACM monolith wall with medium ceramic grains (average grain length around 100 μm with an aspect ratio of 20).

ink, Royal Talens) in the feed of the reactor and recording the exit concentration at various superficial gas velocities and superficial liquid velocities. The superficial gas velocity u_G was varied between 0.01 and 0.22 m/s and the superficial liquid velocity u_L between 0.06 and 0.20 m/s.

A schematic drawing of the experimental setup can be found in Kreutzer et al. [28]. The monolith section with a total length of 94 cm consisted out of six monolith blocks that were stacked on top of each other with a small gap of 2 mm between consecutive monoliths. No attempt was made to align the monolithic channels in the junction between consecutive monoliths. This monolith configuration thus contains five gas–liquid redistribution zones.

Both the inlet and outlet pulse were measured by spectroscopy in the visual range. A detailed description of these measurement techniques can be found in Kreutzer et al. [28]. The reproducibility of the outlet curves was found to be very good. A mass balance over the setup resulted in a difference between the inlet and outlet within 10%.

4. Results

A comparison of representative dimensionless RTD curves ($E(\theta)$-curves) of ACM-L, ACM-LC, ACM-M and cordierite at equal superficial velocities is shown in Fig. 2. The dimensionless breakthrough times of the $E(\theta)$-curves were 0.3 and 0.4 for ACM and cordierite monoliths, respectively. The dimensionless time of the peak maximum was different for the ACM monoliths compared to the cordierite monolith, indicating a different static liquid fraction [28] with ACM-M having the largest static liquid fraction. The cordierite monoliths had a peak maximum of 2 or higher, while that for the ACM monoliths ranged from 1.2 to 1.5 with the ACM-L samples having the lower values. The width of the $E(\theta)$-curves of the cordierite samples was smaller than that of the ACM-M and ACM-L samples. The tailing part was for all $E(\theta)$-curves more or less equal.

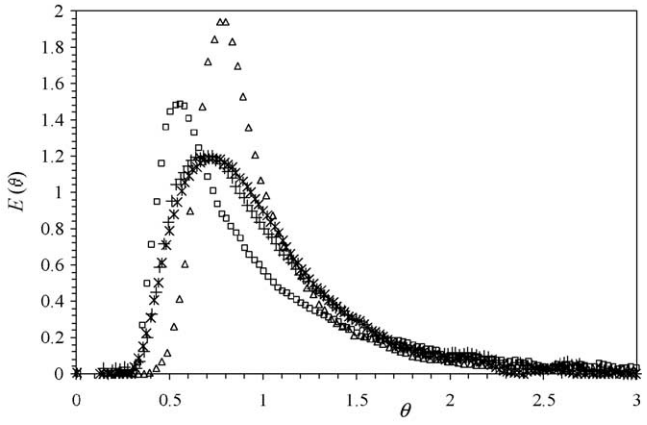

Fig. 2. Representative $E(\theta)$-curves obtained using ACM-M (□), ACM-L (+), ACM-LC (*) and cordierite monoliths (△) for gas–liquid Taylor flow all measured at $u_L = 0.12$ m/s and $u_G = 0.14$ m/s.

The experimentally determined $E(\theta)$-curves were correlated by the piston-dispersion-exchange (PDE) model that is commonly used for fixed bed reactors [29–31]. The numerical details are described in Kreutzer et al. [28]. The PDE model consists of a dynamic liquid zone with axial dispersion and a stagnant liquid zone with mass exchange between the two zones. The PDE model, thus, contains three parameters that characterize the hydrodynamics: (1) the stagnant liquid fraction, *SLF*, that the pulse of tracer exchanges with, located either in the film or within the channel wall, (2) a dimensionless mass transfer parameter N ($N = kaL/((1 - SLF)u_{TP})$, where ka is the mass transfer parameter, L the column length and u_{TP} is the total superficial velocity) that describes how fast tracer in the dynamic liquid zone exchanges with the stagnant liquid and (3) a dimensionless dispersion parameter P that quantifies the extent of maldistribution either being of convective or dynamic origin. The dispersion parameter P is a fit parameter that is used to lump all maldistribution effects.

Some examples of fitted $E(\theta)$-curves are shown in Fig. 3. Most $E(\theta)$-curves could be fitted to the PDE model. Moreover, the fitted PDE curves were checked by careful visual inspection of the fit and the residuals and poor fits were excluded from the following analysis.

Fig. 4 shows the dispersion parameter P as a function of the total liquid holdup ε_L. Fig. 5 shows ka as a function of u_G with u_L constant at 0.14 m/s. Fig. 6 shows the *SLF* as a function of u_{TP}. The drawn lines in Figs. 4–6 merely represent guides to the eye for the PDE parameters. From these figures, it is concluded that the differences between ACM-L and ACM-LC are minimal. Fig. 4 shows a strongly increasing P value with increasing ε_L for cordierite monoliths whereas the P value for the ACM samples is much less or even independent on changes of ε_L. The mean P of the ACM-M and ACM-L monoliths was around 26 and

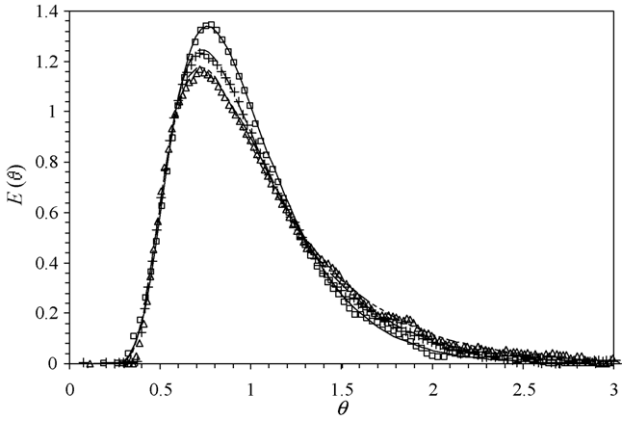

Fig. 3. Examples of $E(\theta)$-curves obtained using ACM-L samples for gas–liquid Taylor flow at various u_L values and u_G values: $u_L = 0.18$ m/s and $u_G = 0.12$ m/s (□), $u_L = 0.13$ m/s and $u_G = 0.13$ m/s (+) and $u_L = 0.11$ m/s and $u_G = 0.21$ m/s (△). The markers represent measured data and the lines represent the fitted data using the PDE model. The best-fit PDE parameters are: $N = 1.1$, $SLF = 0.19$ and $P = 23$ (□); $N = 0.8$, $SLF = 0.20$ and $P = 18$ (+); $N = 0.8$, $SLF = 0.20$ and $P = 14$ (△).

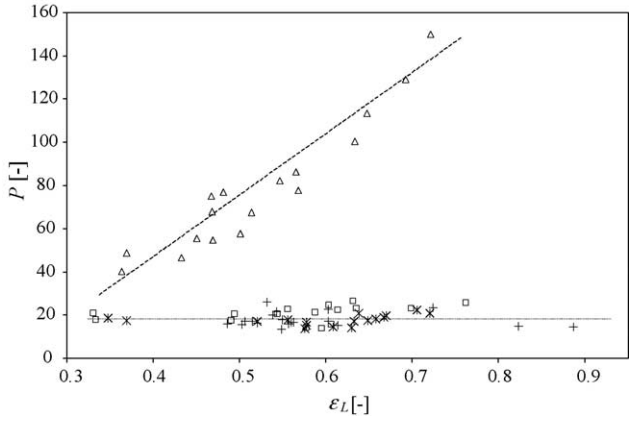

Fig. 4. The dispersion parameter P vs. ε_L for ACM-M (□), ACM-L (+), ACM-LC (*) and cordierite (△). The drawn lines are an indication of the trends.

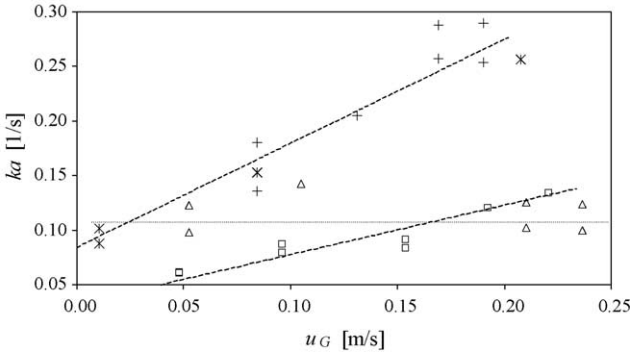

Fig. 5. The mass transfer group ka vs. u_G at constant u_L of 0.14 m/s for ACM-M (□), ACM-L (+), ACM-LC (*) and cordierite (△). The drawn lines are an indication of the trends.

18, respectively. Fig. 5 shows that there is a strong dependence of u_G on ka for ACM-L. The mean value of ka for the ACM-L monolith (0.21) is significantly higher than the mean ka values for the cordierite monolith (0.11) and the ACM-M monolith (0.09). Fig. 6 shows that the *SLF*

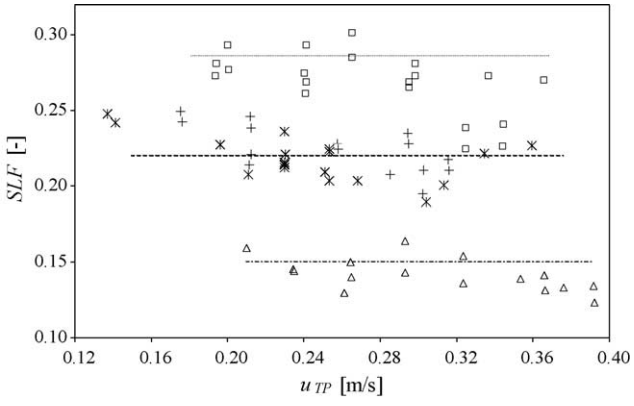

Fig. 6. The static liquid fraction *SLF* as a function of u_{TP} for ACM-M (□), ACM-L (+), ACM-LC (*) and cordierite (△). The drawn lines are an indication of the trends.

is independent on the chosen u_{TP}. The mean *SLF* of ACM-L (and ACM-LC) was 0.22, 0.27 for ACM-M and 0.14 for cordierite.

5. Discussion

5.1. Dispersion parameter

The dimensionless dispersion parameter P as a function of ε_L is depicted in Fig. 4. Larger P values represent more plug flow behavior, thus less peak broadening.

Analysis of frontal photographs of ACM and cordierite samples revealed that the standard deviation of the distribution in channel size was about 20% higher for the ACM samples. Naturally, a channel size distribution leads to a velocity distribution, with higher velocities in the larger channels. If the velocities in the channels are not uniform but Gaussian distributed, then the contribution of the non-uniform velocity to the RTD cannot be distinguished from axial dynamic dispersion inside the channels, as both mechanisms give the same bell-shaped RTD. The difference in channel size distribution alone cannot account for the big difference in P values and the different trends with variation of ε_L (by variation of u_L or u_G) between ACM and cordierite monoliths.

For cordierite monoliths with only one void space between long blocks, it was found that P was primarily determined by the hydrodynamics outside the monolith block, such as the type and position of the distributor and the number of re-distribution zones between blocks [28]. In cordierite, fluid elements cannot 'switch' from a channel with a faster bubble-train flow to a channel with a slow bubble-train flow. As a result, changing the hydrodynamics of the feed zone and the stacking zones by changing ε_L had a noticeable effect on P. This strong dependence of P on ε_L for the cordierite monoliths was not observed for monolith blocks with less void spaces in between [28], so the observed dependence on ε_L is most likely related to the hydrodynamics in the six voids between the short monolith blocks used in this study. Apparently, a low ε_L tends to cause some demixing of gas and liquid in these spaces, while for a sufficiently high ε_L a good redispersion occurs. Hence, the dispersion behavior of the cordierite monoliths used in this study was predominantly influenced by external hydrodynamics.

For the ACM monoliths, fluid elements can – within limits – switch from channels with a fast bubble-train to a channel with a slow bubble-train. This radial dispersion will manifest itself in the RTD as an 'observed' axial dispersion. In any case, the fact that lower P numbers are obtained for ACM must be related to hydrodynamics inside the channels, caused by the higher velocity maldistribution and the higher *SLF* because the distributor and geometry were the same for both ACM and cordierite monoliths. The dissimilar trend of the dispersion behavior for ACM monoliths with variation of the total liquid holdup when compared

with cordierite monoliths showed that the dispersion behavior of ACM monoliths was mostly dominated by internal hydrodynamics.

5.2. Mass transfer parameter

The *ka* values as a function of u_G at constant u_L are given in Fig. 5. A higher *ka* value represents better mass transfer between the dynamic and static liquid zone.

The very open structure of the wall in the ACM-L samples (mean pore size is two times bigger than the ACM-M mean pore size and six times bigger than the cordierite mean pore size) should allow for much faster diffusion inside the wall. Additionally, there is also an effect of the ACM channel wall roughness: the large grains might induce some secondary flow in the film that enhances the mass transfer. Further, the permeable ACM monoliths allow the gas bubbles to push liquid into the wall, adding radial convection to the otherwise only diffusive exchange with the static zone. This is in contrast to gas bubbles in cordierite channels with rather impermeable walls, which can only push the liquid forward, allowing only a small fraction of lubricating film between the bubble and the wall. Fig. 7 shows a schematic representation of this radial convection in an ACM-L monolith. Equating the Laplace bubble pressure with the laminar pressure losses due to flow through the permeable wall (Darcy's law [32]) showed that for all experimental conditions, surface tension could force liquid completely through the ACM-L channel walls. So this suggests that the capillary Laplace pressure of gas bubbles moving through the ACM monolith channels are able to push liquid not only into but completely through the channel walls, adding convection to the otherwise diffusive mass transfer process inside the channels and creating radial liquid transport between adjacent channels. As a result, the reactor volume occupied by the wall participates fully in the ACM-L structures. For the ACM-M, with a four times lower permeability, this was not, or at least to a much lesser extent, the case.

From Fig. 5, one can see that an increase of u_G at constant u_L induced a strong increase of the *ka* of ACM-L (and to a lesser extent also an increase of the *ka* of ACM-M) but did not have an effect on the *ka* of cordierite. An increase in u_G results in longer gas slugs with a longer contact time, which results in a longer pulsating effect. Therefore, a stronger pulsating effect leads to a radial convection contribution that penetrates deeper into the wall and adds more to the overall mass transfer. The increase of u_G also induced higher *ka* values for ACM-M, although for ACM-M the radial convection effect is, as expected, smaller.

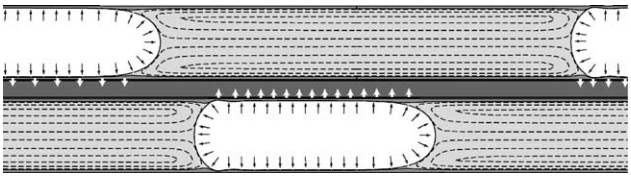

Fig. 7. Schematic representation of gas–liquid Taylor flow in ACM monoliths: a passing liquid bubble pushes the liquid inside the porous ACM wall. The black arrows represent the surface tension forces and the white arrows represent the radial convective transfer of liquid into the ACM walls.

5.3. Static liquid fraction

The *SLF* (*SLF* = liquid film + liquid in wall fraction) is more or less independent on u_{TP} in the measured range (see Fig. 6). The *SLF* of the ACM-L monoliths was about 50% larger than the *SLF* of the cordierite monoliths, while that of the ACM-M monoliths was even about 90% larger. Coating the ACM-L with a thin layer of silica did hardly change its RTD behavior. Only a small delay in the peak maximum of the $E(\theta)$-curve is observed ascribed to the small decrease of porosity of ACM-LC due to the silica coating. The higher *SLF* values of ACM when compared to cordierite are ascribed to the much larger porosity and permeability of the ACM monolith walls. It should be stressed here that the curves were dimensionalized based on the moments of the curve alone, so the amount of column volume occupied by the walls was not explicitly taken into account in any of the curve fits. The *SLF* of the cordierite agrees, within experimental error, with the *SLF* that may be estimated from film thickness correlations for square capillary channels [33]. The higher *SLF* values for ACM-M when compared to ACM-L were due to the much lower permeability of the ACM-M walls. Therefore, the Laplace pressure of the gas slugs was not able to push the liquid out of the wall into an adjacent channel. Moreover, an important additional effect is that when the permeability of the walls is high enough, i.e., for the ACM-L samples, there will be a decrease of the film layer thickness when compared to ACM-M and cordierite.

6. Conclusions

The residence time distribution measurements under Taylor flow conditions show that that the multiphase fluid mechanics are different for cordierite and ACM monoliths. The tracer does not significantly penetrate the macroporous wall of a classical cordierite monolith, but does access the open interior ACM wall. ACM monoliths have higher static liquid fractions when compared to the cordierite structures, i.e., the walls of the ACM monoliths participate in the hydrodynamic process.

The pressure pulse effect of Taylor-bubbles is significant for ACM-L monoliths. For ACM-M, this effect is much less significant. The accessibility of catalyst in the solid structure is greatly enhanced for ACM-L monoliths. Thus, by tailoring the wall morphology of a monolith, one can design more efficient reactors for catalyzed G–L reactions.

The mass transfer parameter of the different ACM monoliths varies, with ACM-L structures having the largest

mass transfer parameter. For the ACM-L monoliths, the mass transfer rate is significantly higher between the liquid bulk and the wall interior than for the classical monolith or for the ACM-M. The grain structure of the ACM-L monoliths influences the hydrodynamic process and there even is interaction between adjacent monolithic channels.

The ability of liquid elements to switch from channel to channel, the higher static liquid fractions and the larger velocity maldistribution induced less plug flow behavior when compared to cordierite monoliths.

Acknowledgements

This work was supported by The Dow Chemical Company. We gratefully acknowledge Dow Core R&D and Corning Inc. for supplying the monolith samples.

References

[1] F. Kapteijn, J.J. Heiszwolf, T.A. Nijhuis, J.A. Moulijn, Cattech 3 (1999) 24.
[2] F. Kapteijn, T.A. Nijhuis, J.J. Heiszwolf, J.A. Moulijn, Catal. Today 66 (2001) 133.
[3] A. Cybulski, J.A. Moulijn, Structured Catalysts and Reactors, Marcel Dekker, New York, 1998.
[4] R.M. Machado, D.J. Parrillo, R.P. Boehme, R.R. Broekhuis, US Patent 6,005,143 (1999).
[5] S. Roy, T. Bauer, M. Al-Dahhan, P. Lehner, T. Turek, AIChE J. 50 (2004) 2918.
[6] J.J. Heiszwolf, L.B. Engelvaart, M.G. van den Eijnden, M.T. Kreutzer, F. Kapteijn, J.A. Moulijn, Chem. Eng. Sci. 56 (2001) 805.
[7] C.N. Satterfield, F. Özel, Ind. Eng. Chem. Fundam. 16 (1977) 61.
[8] M.T. Kreutzer, J.J. Heiszwolf, F. Kapteijn, J.A. Moulijn, C.R. Kleijn, AIChE J., article in press, doi:10.1002/aic.10495.
[9] M.T. Kreutzer, J.J. Heiszwolf, F. Kapteijn, J.A. Moulijn, Chem. Eng. Sci. 25 (2005) 2155–2159.
[10] M.T. Kreutzer, P. Du, J.J. Heiszwolf, F. Kapteijn, F. Moulijn, Chem. Eng. Sci. 56 (2001) 6015.
[11] C.O. Vandu, J. Ellenberger, R. Krishna, Chem. Eng. Proc. 44 (2004) 4999.
[12] J.M. van Baten, R. Krishna, Chem. Eng. Sci. 59 (2004) 2535.
[13] M. Winterbottom, H. Marwan, R. Natividad, Can. J. Chem. Eng. 81 (2003) 838.
[14] T.A. Nijhuis, A.E.W. Beers, T. Vergunst, I. Hoek, F. Kapteijn, J.A. Moulijn, Catal. Rev. 43 (2001) 345.
[15] T. Vergunst, M. Linders, F. Kapteijn, J.A. Moulijn, Catal. Rev. Sci. Eng. 43 (2001) 291.
[16] J.R. Moyer, N.N. Hughes, J. Am. Ceram. Soc. 77 (1994) 1083.
[17] S.A. Wallin, A.R. Prunier, J.R. Moyer, US Patent 6,306,335 (2001).
[18] K. De Lathouder, J.J.W. Bakker, M.T. Kreutzer, F. Kapteijn, J.A. Moulijn, S.A. Wallin, Chem. Eng. Sci. 95 (2004) 5027.
[19] G.I. Taylor, J. Fluid Mech. 10 (1961) 161.
[20] F.P. Bretherton, J. Fluid Mech. 10 (1961) 166.
[21] N. Reinecke, D. Mewes, Int. J. Multiphase Flow 25 (1999) 1373.
[22] M.D. Mantle, A.J. Sederman, L.F. Gladden, S. Raymahasay, J.M. Winterbottom, E.H. Stitt, AIChE J. 48 (2002) 909.
[23] L.F. Gladden, M.H.M. Lim, M.D. Mantle, A.J. Sederman, E.H. Stitt, Catal. Today 79 (2003) 203.
[24] H. Lui, C.O. Vandu, R. Krishna, Ind. Eng. Chem. Res., article in press.
[25] S. Laborie, C. Cabassud, L. Durand-Bourlier, J.M. Lainé, Chem. Eng. Sci. 54 (1999) 5723.
[26] J.J. Heiszwolf, M.T. Kreutzer, M.G. van den Eijnden, F. Kapteijn, J.A. Moulijn, Catal. Today 69 (2001) 51.
[27] G. Berčič, A. Pintar, Chem. Eng. Sci. 52 (1997) 3709.
[28] M.T. Kreutzer, J.J.W. Bakker, F. Kapteijn, J.A. Moulijn, P.J.T. Verheijen, Ind. Eng. Chem. Res. 44 (2005) 4898.
[29] J. Villermaux, W.P.M. van Swaaij, Chem. Eng. Sci. 24 (1969) 1097.
[30] I. Iliuta, F. Thyrion, O. Muntean, M. Giot, Chem. Eng. Sci. 51 (1996) 4579.
[31] D. Stegeman, F.E. van Rooijen, A.A. Kampermans, S. Weijer, K.R. Westerterp, Ind. Eng. Chem. Res. 35 (1996) 378.
[32] J.C. Giddings, Unified Separation Science, Wiley, New York, 1991.
[33] T.C. Thulasidas, M.A. Abraham, R.L. Cerro, Chem. Eng. Sci. 54 (1999) 61.